2014

Mechanistic insights into RNA transphosphorylation from kinetic isotope effects and linear free energy relationships of model reactions

Haoyuan Chen
Rutgers University

Timothy J. Giese
Rutgers University

Ming Huang
Rutgers University

Kin Yiu Wong
Hong Kong Baptist University

Michael E. Harris
Case Western Reserve University School of Medicine

See next page for additional authors

Mechanistic Insights into RNA Transphosphorylation from Kinetic Isotope Effects and Linear Free Energy Relationships of Model Reactions

Haoyuan Chen,[†] Timothy J. Giese,[†] Ming Huang,[†,‡] Kin-Yiu Wong,[¶] Michael E. Harris,[§] and Darrin M. York[*,†]

Center for Integrative Proteomics Research, BioMaPS Institute for Quantitative Biology, and Department of Chemistry and Chemical Biology, Rutgers University, Piscataway, New Jersey 08854, United States, Scientific Computation, University of Minnesota, Minneapolis, Minnesota 55455, United States, Department of Physics, High Performance Cluster Computing Centre, and Institute of Computational and Theoretical Studies, Hong Kong Baptist University, Kowloon Tong, Hong Kong, and Department of Biochemistry, Center for Proteomics and Bioinformatics, Case Western Reserve University School of Medicine, Cleveland, Ohio 44106, United States

E-mail: york@biomaps.rutgers.edu

[*]To whom correspondence should be addressed

[†]Center for Integrative Proteomics Research, BioMaPS Institute for Quantitative Biology, and Department of Chemistry and Chemical Biology, Rutgers University, Piscataway, New Jersey 08854, United States

[‡]Scientific Computation, University of Minnesota, Minneapolis, Minnesota 55455, United States

[¶]Department of Physics, High Performance Cluster Computing Centre, and Institute of Computational and Theoretical Studies, Hong Kong Baptist University, Kowloon Tong, Hong Kong

[§]Department of Biochemistry, Center for Proteomics and Bioinformatics, Case Western Reserve University School of Medicine, Cleveland, Ohio 44106, United States

Abstract

Phosphoryl transfer reactions are ubiquitous in biology, and the understanding of the mechanisms whereby these reactions are catalyzed by protein and RNA enzymes is central to reveal design principles for new therapeutics. Two of the most powerful experimental probes of chemical mechanism involve the analysis of linear free energy relations (LFERs) and the measurement of kinetic isotope effects (KIEs). These experiments provide critical data that reports directly on the characteristics of the rate-controlling transition state, which is the most critical point along the reaction free energy pathway. However, the interpretation of this data in terms of transition state structure and bonding requires the use of theoretical models. In this work, we apply density-functional calculations to determine KIEs for a series of phosphoryl transfer reactions of direct relevance to the 2'-O-transphosphorylation that leads to cleavage of the phosphodiester backbone of RNA. We first examine a well-studied series of phosphate and phosphorothioate mono-, di- and triesters that are useful as mechanistic probes and for which KIEs have been measured. Close agreement is demonstrated between the calculated and measured KIEs, establishing the reliability of our quantum model calculations. Next, we examine a series of RNA transesterification model reactions with a wide range of leaving groups in order to perform, in tandem, analysis of LFERs and KIEs. In this way, we provide a direct connection between the Brønsted coefficients and KIEs with the structure and bonding in the transition state. These relations can be used for prediction or to aid in the interpretation of experimental data for similar non-enzymatic and enzymatic reactions. Finally, we apply these relations to RNA phosphoryl transfer catalyzed by ribonuclease A, and demonstrate the reaction coordinate-KIE correlation is reasonably preserved. These results demonstrate the utility of building up knowledge of mechanism through the systematic study of model systems to provide insight into more complex biological systems such as phosphoryl transfer enzymes and ribozymes.

Introduction

The chemistry of phosphorus is central to many essential biological processes such as cell signaling, energy conversion, and gene regulation.[1–5] Of interest here is the study of phosphoryl transfer reactions in RNA, and in particular, those reactions catalyzed by small prototype RNA and protein enzymes, including the hammerhead,[6] hairpin,[7] hepatitis delta virus,[8] *glmS*[9] and Varkud satellite (VS)[10] ribozymes and RNase A.[11] The mechanisms of phosphoryl transfer reactions, both in enzymatic and non-enzymatic systems, have been studied extensively with experiments. One important method used in those studies is linear free energy relationship (LFER) analysis, which quantifies the effect of changing the nucleophile or leaving group reactivity (via chemical modification) on the reaction rate.[12,13] Brønsted coefficients[14] and Leffler indices[15] are valuable parameters that characterize the extent of bond formation/fission in the rate-controlling transition state (TS) and can be used to discern between pathways through the reaction free energy landscape.[16–20]

Another widely used method in the mechanistic study is the measurement of kinetic isotope effects (KIEs) which are defined as a ratio of rate constants (k_{light}/k_{heavy}) for the light and the heavy isotopically substituted reactions. KIEs arise in part from the difference in the zero point vibrational energies between light and heavy isotopologues and provides an effective approach to specifically probe the bonding pattern in rate-controlling TS.[21,22] Decreased or increased stiffness in the bonding environment surrounding a certain atom in the TS compared to the reactant state leads to a normal (greater than unity) or inverse (less than unity) KIE, respectively, when this atom is substituted by its heavier isotope. Experiments that have been performed to measure KIEs in RNA transphosphorylation have greatly enhanced our understanding of the reaction mechanisms.[23–25]

Although LFER analysis and measurement of KIEs provide critical information that reports on the changes in bonding that occur in the rate-controlling TS, theoretical modeling is required in order to provide a detailed molecular-level interpretation of this data. In the present work, we report results from quantum mechanical calculations of KIEs in series of reactions that are closely related to the RNA transphosphorylation. First, several computational methods for KIE prediction

are tested for a set of benchmark phosphate/phosphorothioate ester hydrolysis reactions[26] which have well-established experimental results. Second, the validated method is applied to a series of RNA transphosphorylation model reactions in which LFERs have been calculated[27] in order to form a quantitative connection with KIE data that can be used for prediction. Finally, model reactions that mimic the RNA phosphodiester backbone cleavage in solution and catalyzed by RNase A[25] are examined and used to aid in the interpretation of experimental KIE measurements, where the reaction coordinate-KIE relationship we obtained from LFER analysis is demonstrated to have predictive value.

Methods

Phosphate/phosphorothioate ester hydrolysis

DFT calculations were performed using both B3LYP[28,29] and M06-2X[30] functionals to establish the appropriate level of theory. Reactant state (RS) and transition state (TS) geometries of the 8 phosphate ester hydrolysis reactions listed in Table 3 of Ref. 26 were optimized using those functionals with 6-31++G(d,p) basis set. PCM solvation model[31,32] was used to address the solvent effects together with two sets of solute atomic radii, UFF[33] and UAKS.[34] Harmonic vibrational analysis was performed to verify the nature of all stationary points. KIEs for those experimentally investigated isotopic substitutions in all 8 reactions were then computed using Bigeleisen equation.[21,35] Temperatures in the KIE calculations were chosen to be consistent with experiments, where relevant.

LFER series

The reverse of dianionic in-line alcoholysis of ethylene phosphate was used in this work as a model for RNA phosphate transesterification reaction (see Scheme 3), as was done in previous work.[24,27] A series of 15 reactions with a wide spectrum of different 5'-O leaving groups (see

Table 2) have been studied. The RS and TS geometries for all reactions were optimized using B3LYP/6-31++G(d,p) in PCM solvation with UAKS radii set. The B3LYP functional was chosen because the B3LYP results from the phosphate ester hydrolysis benchmark calculations described above show better agreement with experiment than those using M06-2X. Nucleophile oxygen (2'-O) and leaving group oxygen (5'-O) KIEs at 298.15K for all reactions were computed by the same method as described in the previous subsection.

RNase A model reactions

RS and TS geometries of the enzymatic model reaction which were optimized with B3LYP/6-31++G(d,p) in PCM implicit solvent using specialized atomic radii for RNase A catalysis, which we've adopted from previous work.[24,25] An additional imidazole ring resembling His12 in RNase A, which was only used in TS in previous work 25, has been added to the RS as well. KIEs of the 2'-O and 5'-O were calculated at 298.15K using the same protocol as described above. All electronic structure calculations were carried out in Gaussian 09 package.[36]

Results and Discussion

Validation and comparison of computed KIEs

Heavy-atom isotope effects, in most cases, have less than a few percent variation from unity.[22] Therefore, it is important to establish a solid computational model which enables the reproduction and prediction of KIE values with satisfactory accuracy. Here, we test three different methods on a related series of phosphate ester hydrolysis reactions[26] in which experimental KIEs have been well established. Scheme 1 shows the structures of all 8 phosphate ester reactants and Scheme 2 illustrates the different types of mechanisms in the hydrolysis of those reactants. The KIEs calculated using the different computational protocols and their corresponding experimental values are listed in Table 1 and displayed in Figure 1. In the hydrolysis of dianionic monoester *p*NPP^{2-},

our calculations suggest a mechanism that agrees with experimental and previous computational results[22,26,37,38] in which the reactant hydrolyzes via a concerted mechanism without an intermediate (Scheme 2, A1). The key bond lengths (P-bridging oxygen: 2.76Å, P-attacking water oxygen: 2.52Å in our B3LYP+UAKS calculation) in the TS we located coincide well with the values from the calculations in Ref. 37 and Ref. 38. For the thio-substituted *p*NPPT^{2-}, we obtain a loose, dissociative transition state (Scheme 2, A2) in which the P-O bond fission is more advanced (P-bridging oxygen: 3.53Å in our B3LYP+UAKS calculation) than in *p*NPP^{2-}, which agrees with the interpretation of KIE experiments in Ref. 26. The computed KIEs for these two reactions are in very good agreement with experimental values. B3LYP produces KIEs that are more consistent with experiment than M06-2X, while application of UAKS radii improves the correlation to experiment relative to UFF radii. For the monoanionic monoester (*p*NPP^{-} and *p*NPPT^{-}) hydrolysis that occur in acidic conditions, experiments in Ref. 26 suggest an advanced but still incomplete proton transfer from the nonbridging oxygen to the leaving group oxygen in the TS. Calculations in the present work support this mechanism (Scheme 2, B). The KIE values given by the different computational models are all reasonably consistent with experiments (see Figure 1 and Table 1).

The other 4 reactions studied in this section involve the alkaline hydrolysis of diesters and triesters. Our calculations suggest an associative mechanism with a tight transition state (having shorter distances to nucleophile and leaving group) for all these reactions (Scheme 2, C & D), in which the leaving group bond cleavage in TS of the diesters are more advanced than of triesters. These conclusions are consistent with various experimental and computational results.[13,19,26,39–42] The computed KIEs show, in general, impressive correlation with experimental values.

Overall, both B3LYP and M06-2X functional give reasonable predictions of KIE values, but the B3LYP results are more consistent with experimental data (correlation coefficient 0.85 vs. 0.73, mean unsigned error 0.0032 vs. 0.0044). The KIE results using UAKS radii generally outperform those using UFF radii (correlation coefficient 0.85 vs. 0.79). Therefore, we choose to use B3LYP density functional with 6-31++G(d,p) basis set and UAKS atomic radii set for the computational model, which will be applied here after to the studies on RNA transphosphorylation model

reactions.

KIEs and LFER in RNA transphosphorylation model reaction series

All the model reactions studied here initiate with the association of the nucleophile involving a pentavalent phosphorane species. There are two associative mechanisms as shown in Scheme 3: a concerted mechanism that passes through a single transition state, and a stepwise mechanism that proceeds via two transition states separated by an intermediate. A concerted mechanism can be classified as synchronous (having similar degrees of bonding to the nucleophile and leaving group in the transition state) and asynchronus (having differing degrees of bonding to the nucleophile and leaving group in the transition state). For either stepwise mechanisms or concerted asynchronus mechanisms, the transition states can be further designated as either "early" or "late", depending on the location of the transition state along a reaction coordinate that involves the difference in leaving group and nucleophile distances with the reactive phosphorus. Specifically, we denote a transition state as being "early" if it is characterized by a small degree of bond formation/cleavage with the nucleophile/leaving group, respectively; a "late" transition state involves a nearly fully formed bond with the nucleophile and a nearly cleaved bond with the leaving group.

Table 2 lists the computed 2'-O and 5'-O KIE values for those reactions as well as the key geometrical information in the rate-limiting TSs and the experimental pK_as of the conjugate acid of those 15 different leaving groups. Figure 2 demonstrates the connection between LFER and KIEs in the characterization of the two classes of mechanisms. Figure 3 shows the correlation between the approximate reaction coordinate $R_2 - R_1$ (R_1 and R_2 stand for the P-O2' and P-O5' bond lengths, respectively) and the KIE values, which will be addressed again in the later discussion on RNase A enzymatic models.

As shown in Figure 2, Figure 3 and Table 2, two distinct groups of KIE values for both 2'-O and 5'-O clearly exist, which correspond to the two types of reaction mechanisms in Scheme 3. For the reactants with poor leaving groups (conjugate acids have relatively high pK_a values, greater than $\approx$ 13), significantly large normal 5'-O KIEs (> 1.03) are observed together with the large in-

verse 2'-O KIEs (< 0.97). These numbers suggest that the P-O2' bonds are almost fully cleaved in the rate-limiting TSs while the P-O5' bonds are nearly fully formed. This is also demonstrated by the positive "reaction coordinate" $R_2 - R_1$ values around 0.55 Å in the rate-limiting TSs (TS2). Early TSs (TS1) can also be located for these reactions but should not be used in the KIE predictions since they are not rate-controlling.[27] Phosphoryl transfer reactions for this type of reactants therefore occur via stepwise mechanisms with late rate-limiting TSs, which agrees with previous experimental and computational studies on closely related systems.[23,24] As for those reactants with enhanced leaving groups (conjugate acids have lower pK_a values, less than $\approx$ 13), the 2'-O KIEs are always large normal while the 5'-O KIEs are mostly normal but much closer to unity. This indicates an early rate-limiting TS in which the P-O2' bond is still forming while the P-O5' bond remains almost uncleaved, which is again supported by the negative $R_2 - R_1$ value. The transphosphorylation process is now shifted to a concerted fashion where the late TSs cannot be located for most reactions in this group as a result of the enhanced leaving groups.

In terms of LFER analysis, as seen in Figure 2, two distinct Brønsted coefficients (β_{lg}s) -1.37 and -0.53 were observed for the two groups of reactants with poor and enhanced and leaving groups, respectively. The β_{lg} value with a much greater magnitude -1.37 for those reactants with poor leaving groups suggests a later rate-limiting TS that involves more P-O5' bond cleavage motion, which makes the reaction rate more sensitive to the change of the leaving group;[27] the β_{lg} with a small magnitude -0.53 for the reactants with sufficiently enhanced leaving groups indicates a concerted mechanism through a single early TS involving mainly P-O2' bond formation motion, which reflects a diminished sensitivity of reaction rate to variation of the leaving group. The break point of pK_a between the two mechanisms is determined to be 13.02 (see Figure 2). From KIE results, we can observe from Table 2 that the pK_a of the break point should fall between 12.37 and 13.55, which coincides very well with the LFER results here and previous reported value 12.58.[43] Hence, we are now able to establish a direct connection between Brønsted coefficients and KIE signatures in the RNA transphosphorylation model reaction series, where both of them give significant indications of the bonding patterns in rate-controlling TSs and agree with each

other.

Application to RNase A enzymatic model

Recently, a combined experimental and theoretical investigation was carried out on the elucidation of RNase A catalytic mechanism via kinetic isotope effects.[25] A simplified reaction model was devised in that work to mimic the RNA 2'-O-transphosphorylation in the enzymatic environment, and the 2'-O and 5'-O KIEs were computed and shown to be consistent with the experimentally measured enzymatic KIEs. Here, the above relationship between $R_2 - R_1$ and KIE values are applied to this model. Optimized RS and TS structures in this model reaction are shown in Figure 4. Although the TS here is still a late one, the 5'-O KIE is less normal than those in the late TSs of LFER series while the 2'-O KIE becomes less inverse, which is well reflected in the more compact TS geometry and less advanced reaction coordinate $R_2 - R_1$ value. More interestingly, computed 2'-O and 5'-O KIEs and $R_2 - R_1$ values in the rate-limiting TS roughly fall on the fitted lines from the LFER series as shown in Figure 3. We can see that the LFER model can be used at least qualitatively to predict the geometrical details for TSs of more complex reactions.

The RNase A data points deviate from the model for several reasons. First of all, the RSs and TSs in the LFER series are all dianionic, which indicates that those reactions occur in basic conditions with the 2'-OH likely deprotonated, while the RNase A reaction model was built to mimic ideal enzymatic condition at pH 7 so the 2'-OH remains protonated in the RS. One could expect the 2'-O KIE value to be more inverse (therefore closer to the line, see Figure 3) without the proton in RS, as the deprotonation process has a normal contribution to the 2'-O KIE while the P-O bond formation contributes inversely.[22,26,44] The addition of sugar rings in the enzymatic model might affect the 2'-O KIE as well since the 2'-OH now becomes a secondary alcohol instead of a primary one and its vibrational modes get coupled with modes of ring. Also, the imidazole ring that mimics the general acid His119 creates a stiffer bonding environment for the 5'-O[25,45,46] in the TS that leads to a decrease in the 5'-O KIE value, which caused greater deviation from the model.

Conclusion

In this work, we present the results of quantum chemical studies on the KIEs in the phosphate ester hydrolysis reactions, non-enzymatic RNA transphosphorylation model reaction series and enzymatic model that represents RNA backbone cleavage catalyzed by RNase A. Benchmark KIE calculations have been performed on the experimentally well-studied phosphate ester hydrolysis system to validate the computational method used for this system. The method that yields most consistent agreement with experiments was identified and then applied to the prediction of KIEs in a model reaction series to establish a relationship between approximate reaction coordinate and 2'-O and 5'-O KIEs. LFER and KIE analysis provide insights from different aspects but eventually converge to the same mechanistic explanation for this system. Finally, KIEs in the RNase A catalysis model are computed and shown to be consistent with the trend observed in the LFER series between KIEs and reaction coordinates. The data presented in this work serves as a useful benchmark and guide to the design and development of next-generation multiscale models for RNA catalysis mechanisms which are of great biological importance.

Acknowledgments

The authors are grateful for financial support provided by the National Institutes of Health (GM62248). Computational resources from the Minnesota Supercomputing Institute for Advanced Computational Research (MSI) were utilized in this work. This work used the Extreme Science and Engineering Discovery Environment (XSEDE), which is supported by National Science Foundation grant number OCI-1053575.

References

(1) Knowles, J. R. *Ann. Rev. Biochem.* **1980**, *49*, 877–919.

(2) Westheimer, F. H. *Science* **1987**, *235*, 1173–1178.

(3) Cleland, W. W.; Hengge, A. C. *Chem. Rev.* **2006**, *106*, 3252–3278.

(4) Cochrane, J. C.; Strobel, S. A. *Acc. Chem. Res.* **2008**, *41*, 1027–1035.

(5) Kamerlin, S. C. L.; Sharma, P. K.; Prasad, R. B.; Warshel, A. *Q. Rev. Biophys.* **2013**, *46*, 1–132.

(6) Scott, W. G.; Murray, J. B.; Arnold, J. R. P.; Stoddard, B. L.; Klug, A. *Science* **1996**, *274*, 2065–2069.

(7) Buzayan, J. M.; Gerlach, W. L.; Bruening, G. *Proc. Natl. Acad. Sci. USA* **1986**, *83*, 8859–8862.

(8) Sharmeen, L.; Kuo, M. Y.; Dinter-Gottlieb, G.; Taylor, J. *J. Virol.* **1988**, *62*, 2674–2679.

(9) Winkler, W. C.; Nahvi, A.; Roth, A.; Collins, J. A.; Breaker, R. R. *Nature* **2004**, *428*, 281–286.

(10) Saville, B. J.; Collins, R. A. *Cell* **1990**, *61*, 685–696.

(11) Raines, R. T. *Chem. Rev.* **1998**, *98*, 1045–1065.

(12) Oivanen, M.; Kuusela, S.; Lönnberg, H. *Chem. Rev.* **1998**, *98*, 961–990.

(13) Lassila, J. K.; Zalatan, J. G.; Herschlag, D. *Annu. Rev. Biochem.* **2011**, *80*, 669–702.

(14) Bronsted, J. N. *Chem. Rev.* **1928**, *5*, 231–338.

(15) Leffler, J. E. *Science* **1953**, *117*, 340–341.

(16) Jencks, D. A.; Jencks, W. P. *J. Am. Chem. Soc.* **1977**, *99*, 7948–7960.

(17) Williams, A. *Acc. Chem. Res.* **1984**, *17*, 425–430.

(18) Bourne, N.; Chrystiuk, E.; Davis, A. M.; Williams, A. *J. Am. Chem. Soc.* **1988**, *110*, 1890–1895.

(19) Onyido, I.; Swierczek, K.; Purcell, J.; Hengge, A. C. *J. Am. Chem. Soc.* **2005**, *127*, 7703–7711.

(20) Hengge, A. C.; Onyido, I. *Curr. Org. Chem.* **2005**, *9*, 61–74.

(21) Bigeleisen, J.; Wolfsberg, M. *Adv. Chem. Phys.* **1958**, *1*, 15–76.

(22) Hengge, A. C. *Acc. Chem. Res.* **2002**, *35*, 105–112.

(23) Harris, M. E.; Dai, Q.; Gu, H.; Kellerman, D. L.; Piccirilli, J. A.; Anderson, V. E. *J. Am. Chem. Soc.* **2010**, *132*, 11613–11621.

(24) Wong, K.-Y.; Gu, H.; Zhang, S.; Piccirilli, J. A.; Harris, M. E.; York, D. M. *Angew. Chem. Int. Ed.* **2012**, *51*, 647–651.

(25) Gu, H.; Zhang, S.; Wong, K.-Y.; Radak, B. K.; Dissanayake, T.; Kellerman, D. L.; Dai, Q.; Miyagi, M.; Anderson, V. E.; York, D. M.; Piccirilli, J. A.; Harris, M. E. *Proc. Natl. Acad. Sci. USA* **2013**, *110*, 13002–13007.

(26) Catrina, I. E.; Hengge, A. C. *J. Am. Chem. Soc.* **2003**, *125*, 7546–7552.

(27) Huang, M.; York, D. M. *Phys. Chem. Chem. Phys.* **2014**, *submitted*.

(28) Becke, A. D. *J. Chem. Phys.* **1993**, *98*, 5648–5652.

(29) Lee, C.; Yang, W.; Parr, R. G. *Phys. Rev. B.* **1988**, *37*, 785–789.

(30) Zhao, Y.; Truhlar, D. G. *Theor. Chem. Acc.* **2008**, *120*, 215–241.

(31) Tomasi, J.; Mennucci, B.; Cammi, R. *Chem. Rev.* **2005**, *105*, 2999–3093.

(32) Scalmani, G.; Frisch, M. J. *J. Chem. Phys.* **2010**, *132*, 114110–114124.

(33) Rappé, A. K.; Casewit, C. J.; Colwell, K. S.; Goddard III, W. A.; Skiff, W. M. *J. Am. Chem. Soc.* **1992**, *114*, 10024–10035.

(34) Barone, V.; Cossi, M.; Tomasi, J. *J. Chem. Phys.* **1997**, *107*, 3210–3221.

(35) Bigeleisen, J.; Mayer, M. G. *J. Chem. Phys.* **1947**, *15*, 261–267.

(36) Frisch, M. J.; Trucks, G. W.; Schlegel, H. B.; Scuseria, G. E.; Robb, M. A.; Cheeseman, J. R.; Scalmani, G.; Barone, V.; Mennucci, B.; Petersson, G. A.; Nakatsuji, H.; Caricato, M.; Li, X.; Hratchian, H. P.; Izmaylov, A. F.; Bloino, J.; Zheng, G.; Sonnenberg, J. L.; Hada, M.; Ehara, M.; Toyota, K.; Fukuda, R.; Hasegawa, J.; Ishida, M.; Nakajima, T.; Honda, Y.; Kitao, O.; Nakai, H.; T., V.; Montgomery, J. A., Jr.; Peralta, J. E.; Ogliaro, F.; Bearpark, M.; Heyd, J. J.; Brothers, E.; Kudin, K. N.; Staroverov, V. N.; Kobayashi, R.; Normand, J.; Raghavachari, K.; Rendell, A.; Burant, J. C.; Iyengar, S. S.; Tomasi, J.; Cossi, M.; Rega, N.; Millam, J. M.; Klene, M.; Knox, J. E.; Cross, J. B.; Bakken, V.; Adamo, C.; Jaramillo, J.; Gomperts, R.; Stratmann, R. E.; Yazyev, O.; Austin, A. J.; Cammi, R.; Pomelli, C.; Ochterski, J. W.; Martin, R. L.; Morokuma, K.; Zakrzewski, V. G.; Voth, G. A.; Salvador, P.; Dannenberg, J. J.; Dapprich, S.; Daniels, A. D.; Farkas, O.; Foresman, J. B.; Ortiz, J. V.; Cioslowski, J.; Fox, D. J. Gaussian 09, Revision A.02. Gaussian, Inc., Wallingford, CT, 2009.

(37) Klähn, M.; Rosta, E.; Warshel, A. *J. Am. Chem. Soc.* **2006**, *128*, 15310–15323.

(38) Zhang, L.; Xie, D.; Xu, D.; Guo, H. *Chem. Commun.* **2007**, *16*, 1638–1640.

(39) Cassano, A. G.; Anderson, V. E.; Harris, M. E. *J. Am. Chem. Soc.* **2002**, *124*, 10964–10965.

(40) Lopez, X.; York, D. M.; Dejaegere, A.; Karplus, M. *Int. J. Quantum Chem.* **2002**, *86*, 10–26.

(41) López-Canut, V.; Ruiz-Pernía, J.; Tuñón, I.; Ferrer, S.; Moliner, V. *J. Chem. Theory Comput.* **2009**, *5*, 439–442.

(42) Hou, G.; Cui, Q. *J. Am. Chem. Soc.* **2012**, *134*, 229–246.

(43) Lönnberg, H.; Strömberg, R.; Williams, A. *Org. Biomol. Chem.* **2004**, *2*, 2165–2167.

(44) Liu, Y.; Gregersen, B. A.; Hengge, A.; York, D. M. *Biochemistry* **2006**, *45*, 10043–10053.

(45) Herschlag, D. *J. Am. Chem. Soc.* **1994**, *116*, 11631–11635.

(46) Formoso, E.; Matxain, J. M.; Lopez, X.; York, D. M. *J. Phys. Chem. B* **2010**, *114*, 7371–7382.

(47) Serjeant, E. P.; Dempsey, B. *Ionisation Constants of Organic Acids in Aqueous Solution*; Pergamon Press: New York, 1979.

(48) Lide, D. R., Ed. *CRC handbook of chemistry and physics*, 90th ed.; CRC Press LLC: Boca Raton, FL, 2010.

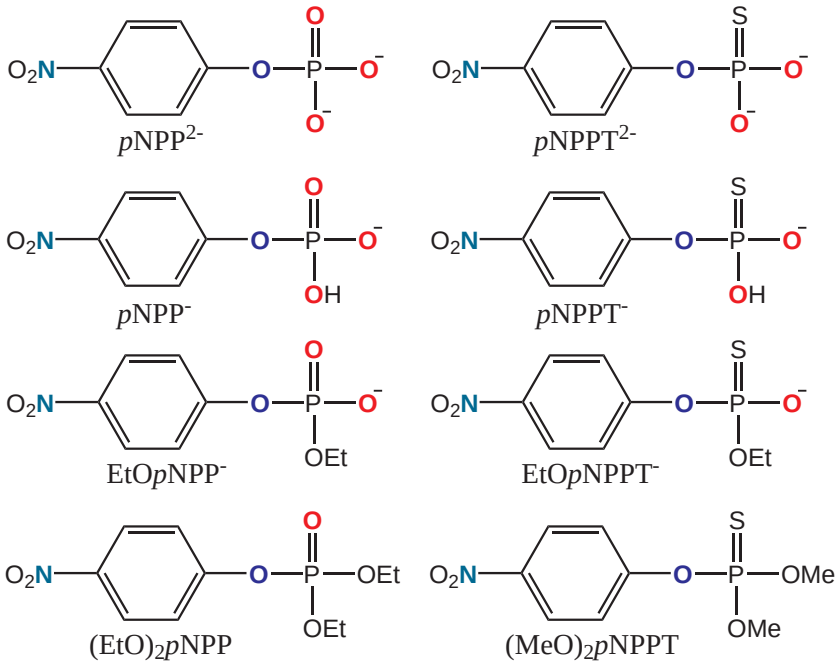

Scheme 1: List of structures and abbreviations of the 8 reactants in the phosphate ester hydrolysis reactions studied in this work. Nitrogen, bridging oxygen and non-bridging oxygen atoms which are colored in dark green, blue and red are used to calculate ^{15}k, $^{18}k_{\text{bridge}}$ and $^{18}k_{\text{nonbridge}}$ values, respectively.

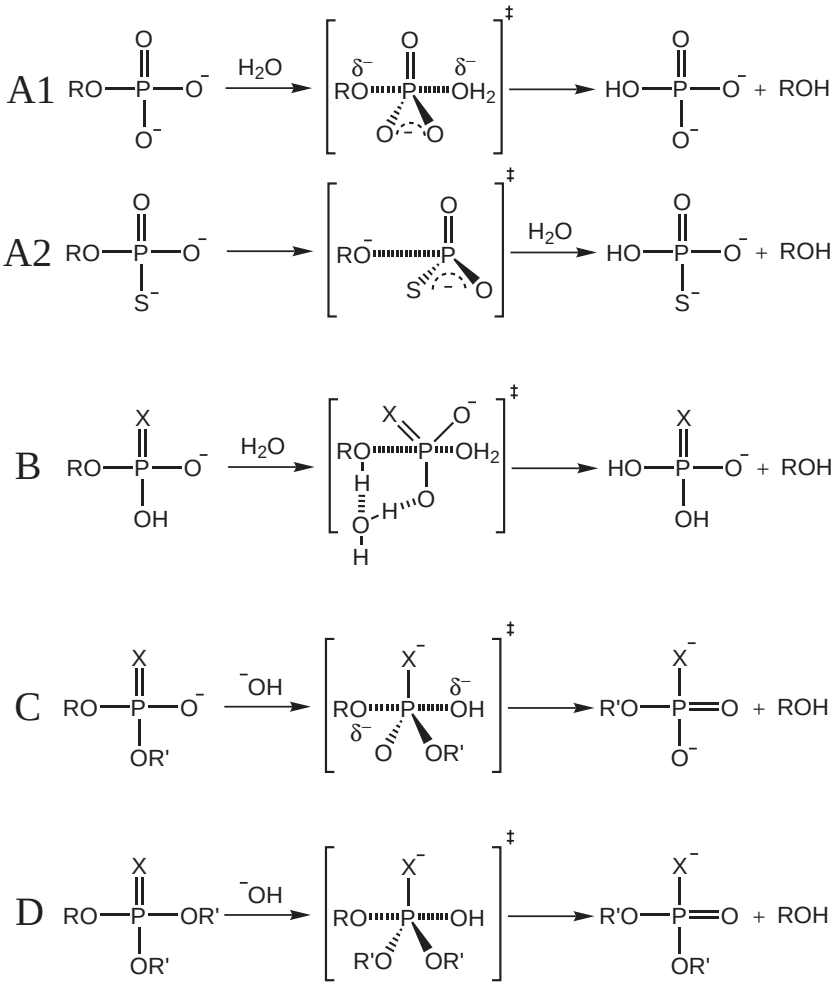

Scheme 2: Illustration of different types of mechanisms in the phosphate ester hydrolysis reactions. A, B, C and D depict the mechanisms with respect to monoester dianionic, monoester monoanionic, diester and triester hydrolysis reactions. R = *p*-nitrobenzene, X = O/S.

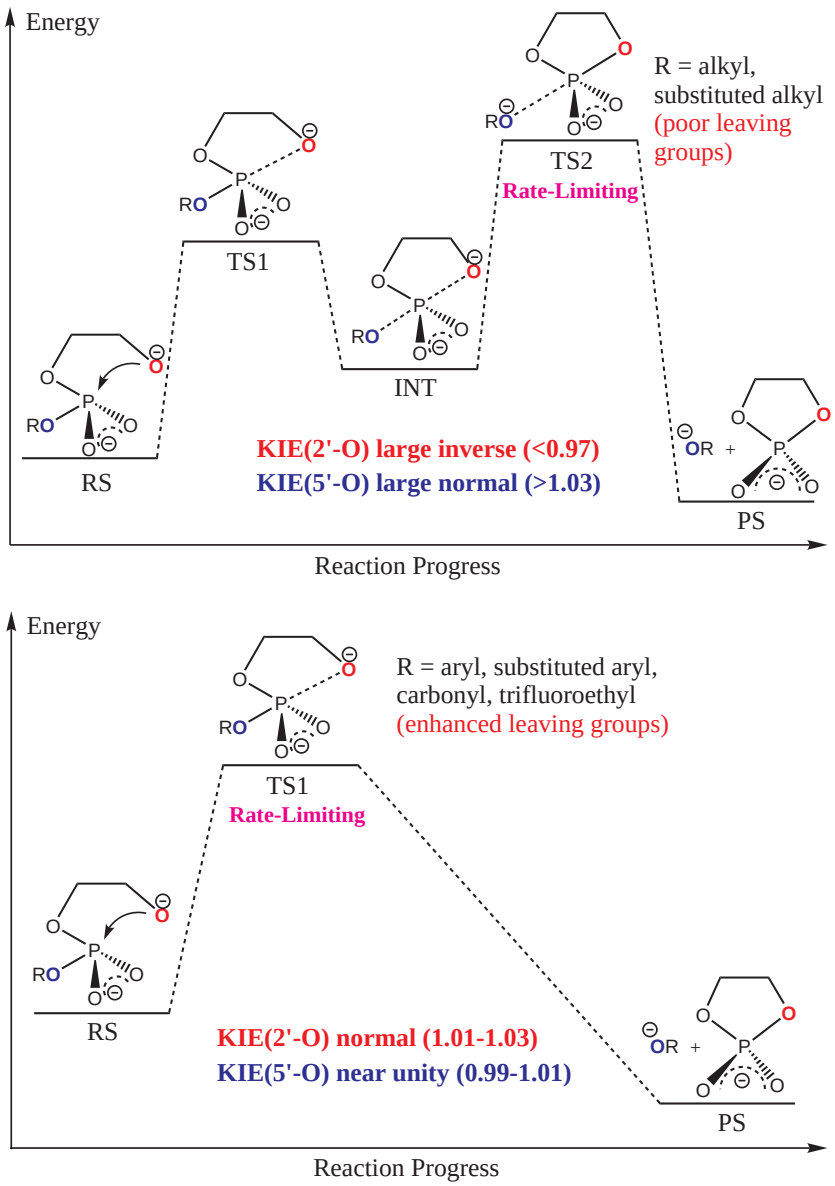

Scheme 3: Illustration of the two types of mechanisms in the LFER series.

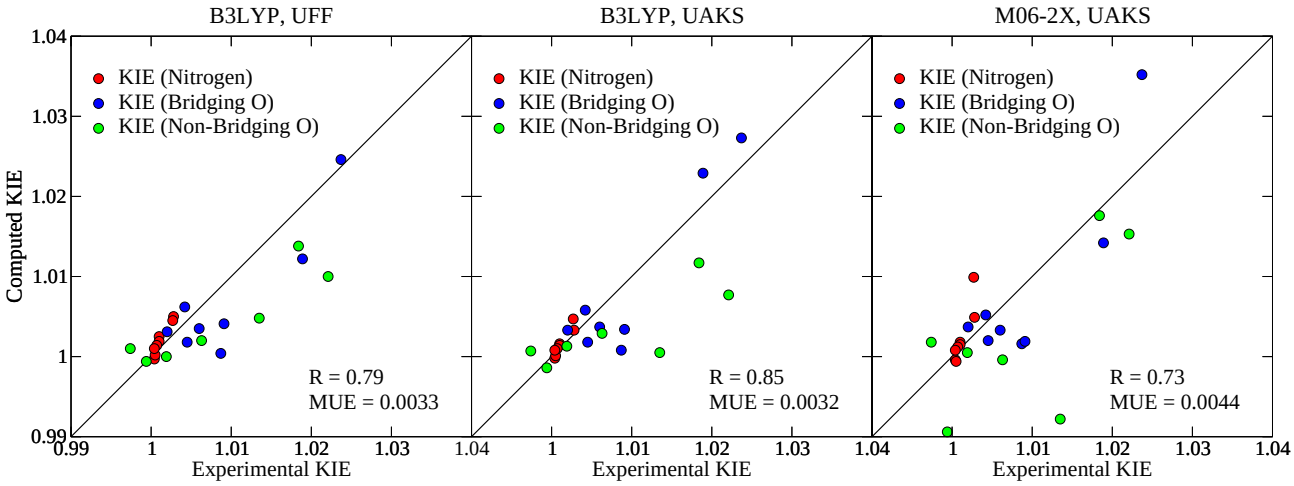

Figure 1: Correlations between computed KIEs using different methods [B3LYP & UFF (left), B3LYP & UAKS (middle) and M06-2X & UAKS (right)] and experimental KIEs in the 8 phosphate ester hydrolysis reactions. Circles in red, blue and green correspond to ^{15}k, $^{18}k_{\text{bridge}}$ and $^{18}k_{\text{nonbridge}}$, respectively.

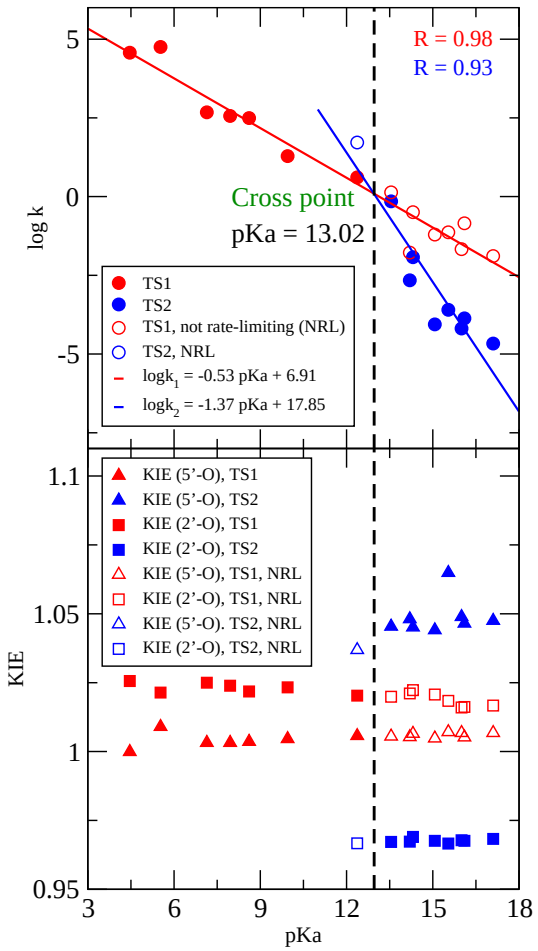

Figure 2: (Top) Linear free energy relationships for early (TS1) and late (TS2) transition states in reverse alcoholysis of ethylene phosphate with different leaving groups. log k values are converted from the calculated reaction barrier and pK_a is the conjugate acid pK_a of the leaving group (data adopted from Ref. 27). (Bottom) Computed 2'-O and 5'-O KIE values for this set of reactions. Filled and unfilled symbols represent the values obtained from rate-limiting and non-rate-limiting transition states, respectively.

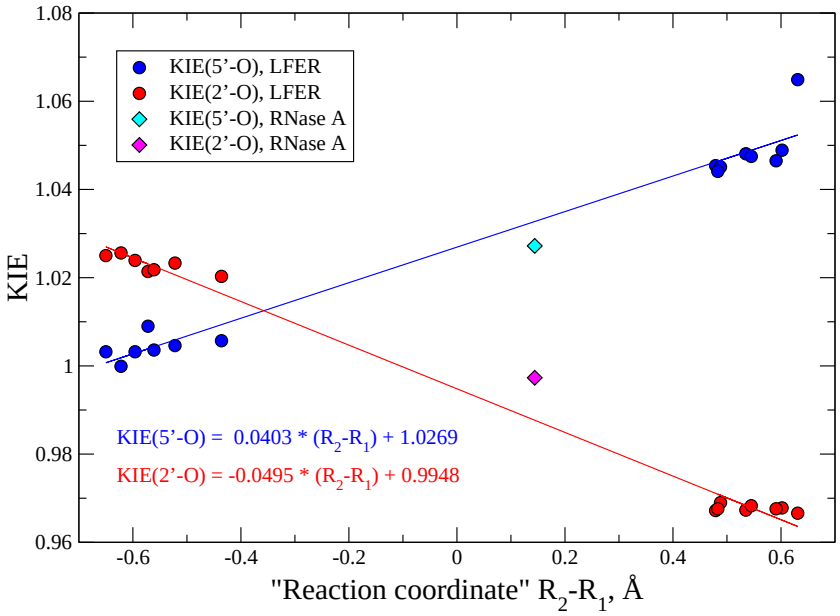

Figure 3: Relationship between computed 2'-O and 5'-O KIE values and key structural information of the rate-limiting TSs in LFER model reactions and RNase A enzymatic model. The points for RNase A (in diamonds) are excluded in the linear fitting.

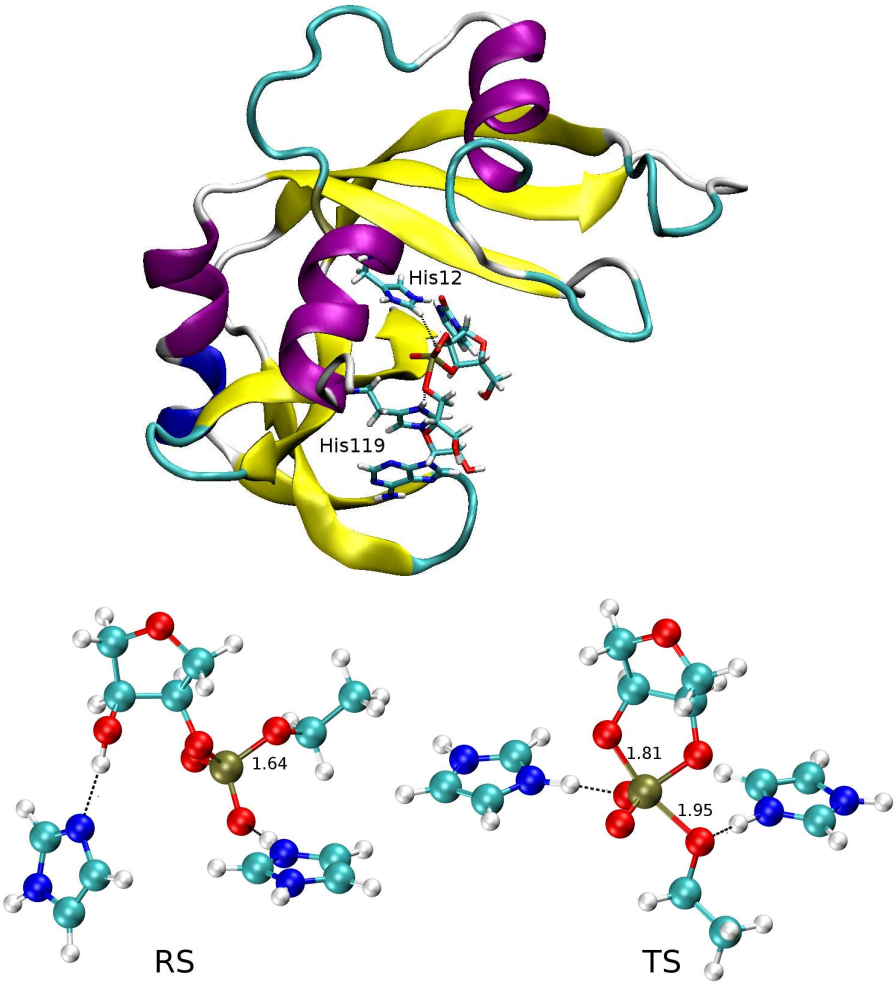

Figure 4: (Top) Structure of RNase A transition state mimic, in which His12 stablizes the negative charges on the non-bridging oxygens and His119 acts as a general acid to facilitate P-O5' bond cleavage. (Bottom) Reactant state (left) and transition state (right) structures in the model reaction. The two imidazole rings in the RS and TS structures are used to mimic His12 (left) and His119 (right). Key bond lengths (in Å) are labeled.

Table 1: Comparison of KIE values for phosphate/phosphorothioate ester hydrolysis reactions. Most experimental results are from Ref. 26 while the $^{18}k_{\mathbf{nonbridge}}$ value for EtO*p*NPP$^-$ (0.9974) comes from Ref. 13. Structures and abbreviations of all reactants are shown in Scheme 1. Different classes of mechanisms are illustrated in Scheme 2. $^{18}k_{\mathbf{nonbridge}}$ values for the hydrolysis of $(\mathbf{MeO})_2$*p*NPPT are not applicable because there is no non-bridging oxygen in this reactant. Numbers in parentheses are the signed errors multiplied by 10^4. R is Pearson's correlation coefficient, MSE and MUE stand for mean signed error and mean unsigned error, respectively.

Reactant (Mechanism)	Substitution	B3LYP		M06-2X	Expt.
		UFF	UAKS	UAKS	
*p*NPP^{2-}(95°C)	^{15}k	1.0033 (+5)	1.0050 (+22)	1.0049 (+21)	1.0028
(A1)	$^{18}k_{\text{bridge}}$	1.0229 (+40)	1.0122 (-67)	1.0142 (-47)	1.0189
	$^{18}k_{\text{nonbridge}}$	0.9986 (-8)	0.9994 (0)	0.9906 (-88)	0.9994
*p*NPPT^{2-}(50°C)	^{15}k	1.0047 (+20)	1.0045 (+18)	1.0099 (+72)	1.0027
(A2)	$^{18}k_{\text{bridge}}$	1.0273 (+36)	1.0246 (+9)	1.0352 (+115)	1.0237
	$^{18}k_{\text{nonbridge}}$	1.0005 (-130)	1.0048 (-87)	0.9922 (-213)	1.0135
*p*NPP$^-$(95°C)	^{15}k	0.9998 (-6)	0.9997 (-7)	0.9996 (-8)	1.0004
(B)	$^{18}k_{\text{bridge}}$	1.0008 (-79)	1.0004 (-83)	1.0016 (-71)	1.0087
	$^{18}k_{\text{nonbridge}}$	1.0117 (-67)	1.0138 (-46)	1.0176 (-8)	1.0184
*p*NPPT$^-$(30°C)	^{15}k	1.0001 (-4)	1.0002 (-3)	0.9994 (-11)	1.0005
(B)	$^{18}k_{\text{bridge}}$	1.0034 (-57)	1.0041 (-50)	1.0019 (-72)	1.0091
	$^{18}k_{\text{nonbridge}}$	1.0077 (-144)	1.0100 (-121)	1.0153 (-68)	1.0221
EtO*p*NPP$^-$(95°C)	^{15}k	1.0016 (+6)	1.0025 (+15)	1.0018 (+8)	1.0010
(C)	$^{18}k_{\text{bridge}}$	1.0058 (+16)	1.0062 (+20)	1.0052 (+10)	1.0042
	$^{18}k_{\text{nonbridge}}$	1.0007 (+33)	1.0010 (+36)	1.0018 (+44)	0.9974
EtO*p*NPPT$^-$(95°C)	^{15}k	1.0014 (+4)	1.0019 (+9)	1.0015 (+5)	1.0010
(C)	$^{18}k_{\text{bridge}}$	1.0033 (+13)	1.0031 (+11)	1.0037 (+17)	1.0020
	$^{18}k_{\text{nonbridge}}$	1.0013 (-6)	1.0000 (-19)	1.0005 (-14)	1.0019
$(\text{EtO})_2$*p*NPP(25°C)	^{15}k	1.0010 (+3)	1.0014 (+7)	1.0012 (+5)	1.0007
(D)	$^{18}k_{\text{bridge}}$	1.0037 (-23)	1.0035 (-25)	1.0033 (-27)	1.0060
	$^{18}k_{\text{nonbridge}}$	1.0029 (-34)	1.0020 (-43)	0.9996 (-67)	1.0063
$(\text{MeO})_2$*p*NPPT(30°C)	^{15}k	1.0008 (+4)	1.0010 (+6)	1.0008 (+4)	1.0004
(D)	$^{18}k_{\text{bridge}}$	1.0018 (-27)	1.0018 (-27)	1.0020 (-25)	1.0045
R		0.79	0.85	0.73	
MSE		-0.0018	-0.0018	-0.0018	
MUE		0.0033	0.0032	0.0044	

Table 2: Computed KIE values for LFER reactions and RNase A model reaction. Experimental pK_as of the conjugate acids of different leaving groups are taken from IUPAC chemical data series, No. 23,[47] except for $HOCH_2CH_2OH$ and 2,3,5,6-F_4-C_6HOH, which are obtained from CRC Handbook[48] and Bourne *et al.*,[18] respectively. R_1 and R_2 denote for the distances (in Å) from phosphorous atom to 2'-oxygen atom and 5'-oxygen atom, respectively, in the optimized structure of the rate-limiting transition states. RNase A experimental KIEs were measured at 310.15K[25] instead of 298.15K for all other KIEs. Numbers in parentheses are the standard deviations for experimentally measured KIEs.

Leaving Group	Expt. pK_a	$R_2 - R_1$	KIE(2'-O)	KIE(5'-O)
CH_3COO^-	4.46	-0.62	1.0256	0.9999
2,3,5,6-F_4-C_6HO^-	5.53	-0.57	1.0214	1.0090
4-NO_2-$C_6H_4O^-$	7.14	-0.65	1.0250	1.0032
4-CN-$C_6H_4O^-$	7.95	-0.60	1.0239	1.0032
3-CN-$C_6H_4O^-$	8.61	-0.56	1.0218	1.0036
$C_6H_5O^-$	9.95	-0.52	1.0233	1.0046
$CF_3CH_2O^-$	12.37	-0.44	1.0203	1.0057
$HCCCH_2O^-$	13.55	0.48	0.9672	1.0454
$FCH_2CH_2O^-$	14.2	0.54	0.9673	1.0481
$ClCH_2CH_2O^-$	14.31	0.49	0.9690	1.0451
$HOCH_2CH_2O^-$	15.07	0.48	0.9676	1.0441
CH_3O^-	15.54	0.63	0.9666	1.0649
$CH_3CH_2O^-$	16	0.60	0.9678	1.0489
$CH_3CH_2CH_2O^-$	16.1	0.59	0.9676	1.0465
$CH_3CH_3CHO^-$	17.1	0.55	0.9683	1.0475
RNase A Model		0.14	0.9973	1.0272
RNase A Expt.		N/A	0.994(2)	1.014(3)

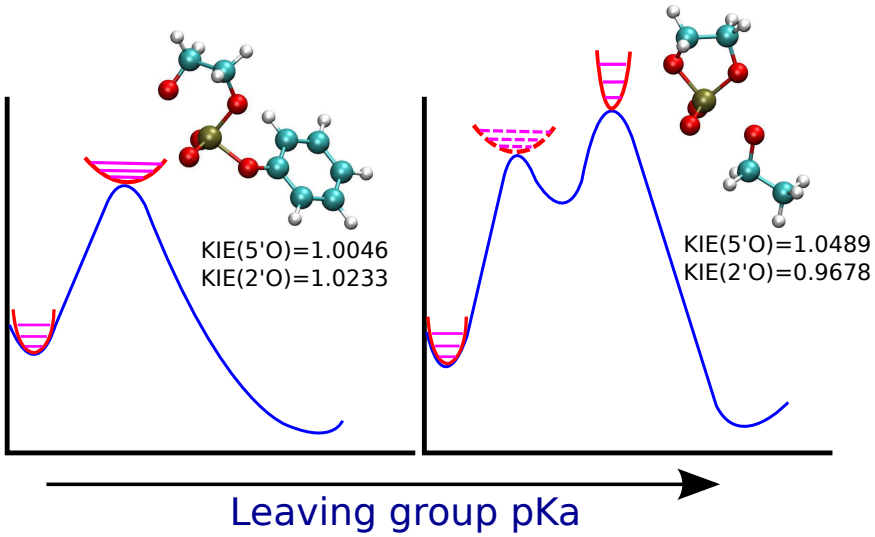

Figure 5: Table of Contents